Science
AAAS

Mg/Al Ordering in Layered Double Hydroxides Revealed by Multinuclear NMR Spectroscopy

Paul J. Sideris, *et al.*

Science **321**, 113 (2008);
DOI: 10.1126/science.1157581

Science (print ISSN 0036-8075; online ISSN 1095-9203) is published weekly, except the last week in December, by the American Association for the Advancement of Science, 1200 New York Avenue NW, Washington, DC 20005.

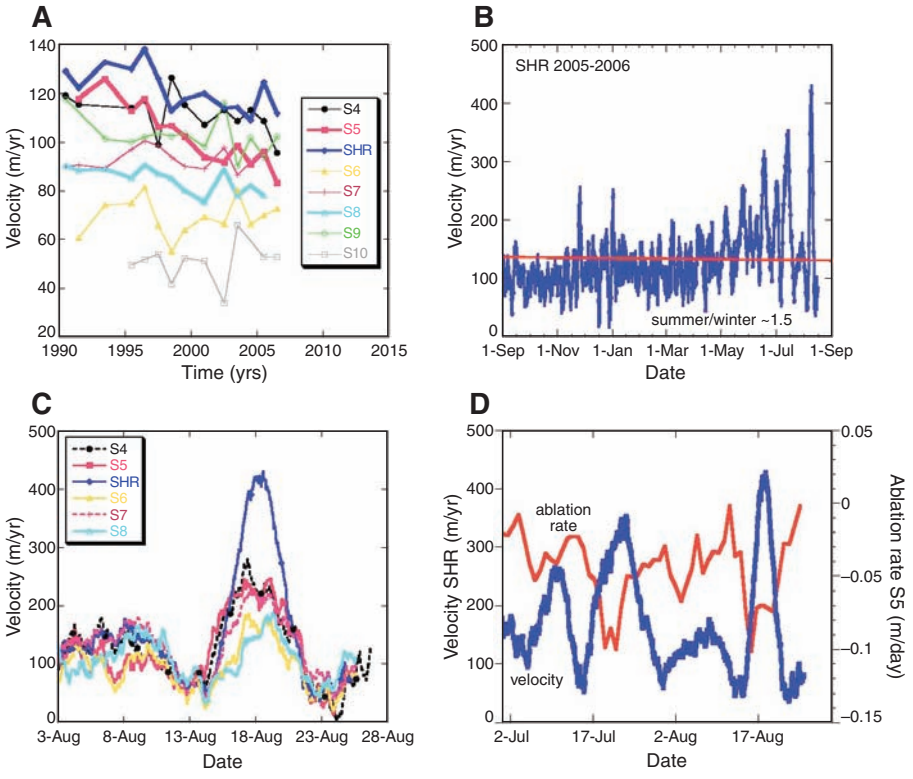

Fig. 3. (**A**) Variations in annual velocity along the K-transect over 17 years; sites with a significant decrease over time are depicted as thick lines. (**B** and **C**) Summer velocities at SHR are about 50% higher than winter velocities (B), which are in phase along the entire transect, particularly at the end of the melt season (C). (**D**) The changes in velocity are clearly related to the ablation rate. If the ablation rate increases, more meltwater is present and velocities increase; however, if ablation ceases, velocities decrease again. This implies that the change in meltwater, rather than the absolute amount of meltwater, determines the change of the velocity within a season.

Longer observational records with high temporal resolution in other ablation areas of the ice sheet are necessary to test the importance of the positive-feedback mechanism between melt rates and ice velocities. At present, we cannot conclude that this feedback is important. We do see a significant increase of the ablation rate (Fig. 2), which is likely related to climate warming, but it remains to be seen if this is likely to be amplified by increasing annual ice velocities.

References and Notes

1. W. Abdalati *et al.*, *J. Geophys. Res.* **106**, 33729 (2001).
2. E. Rignot, P. Kanagaratnam, *Science* **311**, 986 (2006).
3. L. A. Stearns, G. S. Hamilton, *Geophys. Res. Lett.* **34**, L05503 (2007).
4. P. Lemke *et al.*, in *Climate Change 2007*: *The Physical Science Basis. Contribution of Working Group 1 to the Fourth Assessment Report of the Intergovernmental Panel on Climate Change*, S. Solomon *et al.*, Eds. (Cambridge Univ. Press, Cambridge, 2007), pp. 337–383.
5. I. M. Howat, I. Joughin, T. A. Scambos, *Science* **315**, 1559 (2007).
6. W. B. Krabill *et al.*, *Geophys. Res. Lett.* **31**, L24402 (2004).
7. H. J. Zwally *et al.*, *Science* **297**, 218 (2002).
8. I. Joughin *et al.*, *Science* **320**, 781 (2008).
9. R. S. W. van de Wal, W. Greuell, M. R. van den Broeke, C. H. Reijmer, J. Oerlemans, *Ann. Glaciol.* **42**, 311 (2005).
10. T. Vincenty, *Surv. Rev.* **23**, 88 (1975).
11. S. B. Das *et al.*, *Science* **320**, 778 (2008).
12. C. J. van der Veen, *Geophys. Res. Lett.* **34**, L01501 (2007).
13. A. Iken, R. A. Bindschadler, *J. Glaciol.* **32**, 101 (1986).
14. T. C. Bartholomaus, R. A. Anderson, S. P. Anderson, *Nat. Geosci.* **1**, 33 (2008).

15. This work was supported by several grants from the Netherlands Organization of Scientific Research and the Netherlands Polar Programme.

1 April 2008; accepted 5 June 2008
10.1126/science.1158540

Mg/Al Ordering in Layered Double Hydroxides Revealed by Multinuclear NMR Spectroscopy

Paul J. Sideris,[1,2] Ulla Gro Nielsen,[1,2]* Zhehong Gan,[3] Clare P. Grey[1,2]†

The anion-exchange ability of layered double hydroxides (LDHs) has been exploited to create materials for use in catalysis, drug delivery, and environmental remediation. The specific cation arrangements in the hydroxide layers of hydrotalcite-like LDHs, of general formula $Mg^{2+}_{1-x}Al^{3+}_{x}OH_2(Anion^{n-}_{x/n})\cdot yH_2O$, have, however, remained elusive, and their elucidation could enhance the functional optimization of these materials. We applied rapid (60 kilohertz) magic angle spinning (MAS) to obtain high-resolution hydrogen-1 nuclear magnetic resonance (^{1}H NMR) spectra and characterize the magnesium and aluminum distribution. These data, in combination with ^{1}H-^{27}Al double-resonance and ^{25}Mg triple-quantum MAS NMR data, show that the cations are fully ordered for magnesium:aluminum ratios of 2:1 and that at lower aluminum content, a nonrandom distribution of cations persists, with no Al^{3+}-Al^{3+} close contacts. The application of rapid MAS NMR methods to investigate proton distributions in a wide range of materials is readily envisaged.

Hydrotalcite-like layered double hydroxides (LDHs) are a class of inorganic lamellar compounds with the general chemical composition $M^{2+}_{1-x}M^{3+}_{x}(OH)_2(A^{n-}_{x/n})\cdot yH_2O$, where M^{2+} and M^{3+} are divalent and typically trivalent metal cations respectively, x is the molar ratio of the trivalent cation $[M^{3+}/(M^{2+} + M^{3+})]$, which typically varies between 17% and 33% (*1*), and A^{n-} is an anion with charge n. The presence of a trivalent metal in the metal hydroxide $[M_{1-x}M'_x(OH)_2]$ sheet induces an overall positive charge, which is compensated by the incorporation of the anion, along with structural water, in the interlayer spaces (Fig. 1). One naturally occurring example of this class of materials is the mineral hydrotalcite, $Mg_6Al_2(OH)_{16}CO_3\cdot 4H_2O$, which contains carbonate ions in between the layers. The materials can accommodate a wide range of different anions (*2*) and cations (*3*), leading to a large compositional variety and thus tunability for a large number of applications.

These materials are of considerable geological relevance because of their anion-exchange capacity, which can affect the mobility of chemical species in the environment. Although there is a large group of materials with cation-exchange capabilities, the number of systems with positively charged frameworks or layers is extremely limited. LDHs are, therefore, attractive candidates as anion exchangers and can be used, for example, to remove toxic anions such as chromates (*4*), selenates (*5*), or halides (*6*) from waste waters or, more recently, as drug delivery systems (*7*). The materials are also frequently used as catalysts, catalyst supports, or precursors for oxides

used in numerous reactions (*1*, *8*). Organic polymers have been incorporated into LDHs through direct exchange or in situ polymerization from exchanged monomers in the interlayers, creating nanocomposite materials with improved thermal properties (*9*).

An understanding of the basis for the varying anion selectivities of different LDHs requires a molecular-level understanding of the modes of anion binding of the anions within the interlayer spaces. Such insight requires determination of both the structures in the interlayer region and the cation arrangements in the layers themselves, as the latter will control the charge distributions of the hydroxyl groups that point into the interlayer region. Diffraction techniques are not well suited for structural studies of the most prevalent LDHs, namely those containing Mg and Al, for three reasons. First, Mg and Al have effectively identical scattering power, making them indistinguishable by x-ray diffraction. Second, the challenge of synthesizing fully deuterated LDHs, with extremely low residual proton contents, hinders high-resolution neutron studies. Third, many LDHs show considerable turbostratic disorder and stacking faults, complicating the analysis of the diffraction patterns (*10*, *11*).

Nuclear magnetic resonance (NMR) studies of LDHs are particularly attractive due to an abundance of spin-active nuclei from which site-specific structural information can be potentially extracted. However, the high concentration of interlayer water and hydroxyl groups results in strong ^{1}H homonuclear coupling, which broadens the resonances and prevents both ready identification and quantification of chemically distinct ^{1}H environments, particularly at spinning speeds below 25 kHz (*12*–*14*). ^{27}Al magic angle spinning (MAS) NMR studies of hydrotalcite-like LDHs are the most common and have been used to examine thermal decomposition; however, no clear-cut evidence for cation distributions has emerged from these studies (*15*).

Studies using ^{25}Mg MAS NMR spectroscopy are not routine because of this isotope's low gyromagnetic ratio (which determines sensitivity), low natural abundance (~10%), and large quadrupole moment (which broadens the resonances through the interaction with the local electric-field gradient at the site of the nucleus). Nevertheless, the large quadrupole moment provides a very sensitive probe of the variations in the local environment around Mg, and correlations have, for example, been found between the distortions of the bond angles from perfect octahedral symmetry and the quadrupolar coupling constant C_Q (*16*). Single-pulse ^{25}Mg MAS NMR spectra have been collected for hydrotalcite (*16*, *17*) and the related mineral brucite [$Mg(OH_2)$] (*18*–*20*), in which tri-octahedral metal hydroxide sheets are occupied solely by Mg. The introduction of Al into brucite-like metal hydroxide sheets produces distortions in the layer, resulting in a significant increase in the electric-field gradient measured at the Mg site. Although the spectra of both minerals could be simulated with a model that assumed only one site geometry [yielding δ_{iso} = 10 parts per million (ppm), C_Q = 4.4 MHz, and δ_{iso} = 13.5 ppm, C_Q = 3.15 MHz, for hydrotalcite and brucite, respectively], it was not clear from this study whether all the different Mg local environments, some of which could be present in low concentrations, were resolved.

Here, we report the results from a combined ^{1}H and ^{25}Mg NMR investigation of three LDHs containing 19%, 25%, and 33% Al [MgAl-19, MgAl-25, and MgAl-33, respectively (*21*)]. Two recent advances in NMR techniques and instrumentation are applied, which noticeably improve the resolution of the spectra acquired from these materials, providing unambiguous evidence for complete cation ordering in the 33% Al doped sample, and a nonrandom distribution of cations in the lower Al-content materials. First, we make use of a MAS NMR probe that is capable of achieving extremely rapid MAS frequencies of up to 60 kHz. At low spinning speeds, broad featureless spectra result because of the large ^{1}H homonuclear dipolar couplings between the OH groups and occluded water molecules (*22*). However, by using MAS frequencies of above 40 kHz, these dipolar couplings are almost completely removed, allowing the individual H sites to be resolved in these high-proton-content materials. Second, we apply two-dimensional (2D) triple-quantum (TQ) ^{25}Mg MAS NMR techniques (*23*–*25*) to remove the broadening due to the second-order quadrupole interaction. This 2D echo method produces high-resolution spectra—by making use of the different sizes of the second-order quadrupolar interactions in the TQ and single-quantum dimensions of a half-integer spin nucleus such as ^{25}Mg (*26*)—and can be used to reveal multiple sites not evident in the broader 1D spectra. The chosen sample stoichiometries investigated here are representative of low, medium, and high Al content samples, allowing the degree of cation ordering to be explored as a function of Al concentration. Nitrate-containing LDHs are investigated rather than the mineral hydrotalcite, because these materials can then be used for subsequent ion-exchange studies: The carbonate groups in hydrotalcite are not readily exchanged (*27*). However, the approaches demonstrated here can be applied to any Mg- and Al-containing LDHs, and to investigate OH/H_2O environments in a much wider range of minerals.

Once peak broadening is minimized, ^{1}H MAS NMR spectroscopy, in principle, provides a simple method for monitoring cation ordering. Because every hydroxyl group in the LDH layer is coordinated to three metals (each either Mg or Al), four hydroxyl local environments, and thus four distinct ^{1}H resonances, are possible: Mg_3-OH, Mg_2Al-OH, $MgAl_2$-OH, and Al_3-OH (Fig. 1). Assuming a random distribution of the metals on the metal hydroxide sheets, the binomial distribution formula (see SOM text for details) can be used to calculate the percentage of each hydroxyl

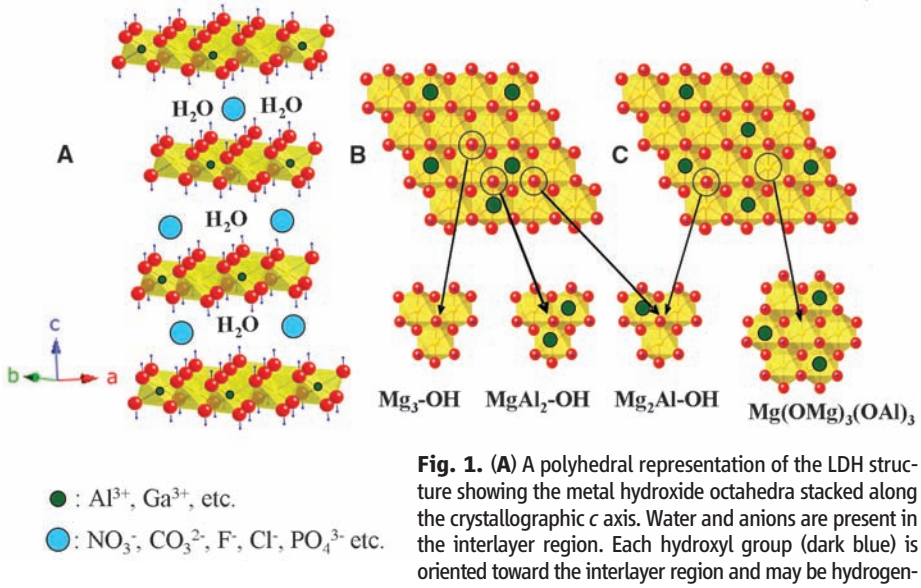

Fig. 1. (**A**) A polyhedral representation of the LDH structure showing the metal hydroxide octahedra stacked along the crystallographic *c* axis. Water and anions are present in the interlayer region. Each hydroxyl group (dark blue) is oriented toward the interlayer region and may be hydrogen-bonded to the interlayer anions and water. The metal hydroxide sheets of an LDH with a Mg:Al ratio of 2:1 are shown with (**B**) random and (**C**) ordered cation distributions. Three major classes of hydroxyl groups are present in (B) (Mg_3-OH, Mg_2Al-OH, and $MgAl_2$-OH), whereas only one hydroxyl environment (Mg_2Al-OH) and one Mg local environment [$Mg(OMg)_3(OAl)_3$] are present in (C).

[1]Department of Chemistry, Stony Brook University, Stony Brook, NY 11794–3400, USA. [2]Center for Environmental Molecular Sciences, Stony Brook University, Stony Brook, N 11794–3400, USA. [3]Center of Interdisciplinary Magnetic Resonance, National High Magnetic Field Laboratory, Tallahassee, FL 32310, USA.

*Present address: Department of Physics and Chemistry, University of Southern Denmark, Campusvej 55, 5230 Odense M, Denmark.

†To whom correspondence should be addressed. E-mail: cgrey@notes.cc.sunysb.edu

resonance as a function of Al content (Table 1). Figure 2A shows the dramatic effect of spinning speed on the resolution of the ^{1}H MAS NMR spectrum of MgAl-33. Three distinct ^{1}H resonances are clearly resolved, which may be readily quantified, when spinning speeds above 40 kHz are used. The relative intensities of these resonances, and their chemical shifts, vary as a function of Al content (Fig. 2B), but the number of distinct resonances remains constant. This observation stands in stark contrast to the random distribution model, which predicts that a total of four hydroxyl groups, and at least one water resonance, will be present.

The spectrum of MgAl-19 shows three ^{1}H resonances at 0.8, 2.4, and 4.7 ppm (Fig. 2B). The chemical shift of the 4.7-ppm resonance is consistent with water occluded in the interlayers (*22*). At low Al concentrations, the two hydroxide environments Mg_3-OH and Mg_2Al-OH should predominate. Given the ~0 ppm chemical shift of the dominant ^{1}H resonance in brucite, which contains only one proton local environment (Mg_3-OH), the resonance at 0.8 ppm is similarly assigned to this local environment. The presence of an Al atom increases the acidity of the hydroxyl group, which results in a shift to higher frequencies (i.e., downfield) (*28*), and on this basis, the peak at 2.4 ppm is assigned to the Mg_2Al-OH group. This resonance shifts gradually to higher frequency as the Al content is increased, which is consistent with stronger hydrogen bonding to the interlayer anions and water with increasing charge on the hydroxide layers. The shift of the Mg_2Al-OH resonance is accompanied by a decrease in the intensity of the 0.8 ppm (Mg_3-OH) resonance, consistent with its assignment. Two-dimensional magnetization exchange experiments (*29*) were performed at a MAS frequency of 60 kHz to explore whether any motion is present in these systems. The experiments reveal that, although slow exchange processes involving exchange between the different OH and H_2O molecules do occur (see SOM text), which are more pronounced for the lower Al-content samples, these do not occur on a time scale that is fast enough to affect the chemical shift positions and intensities of the ^{1}H resonances. Some residual ^{1}H line broadening of the resonances may result from these processes, particularly in the lower Al-content sample MgAl-19.

A large discrepancy exists between the measured relative intensities of the hydroxyl group resonances in the LDH spectra and those calculated assuming the random distribution model, especially for the compound with the greatest Al content, MgAl-33 (Table 1). In particular, no local environments containing more than one Al (e.g., $MgAl_2$-OH and Al_3-OH) are observed, which provides clear evidence that there are no Al^{3+}-Al^{3+} contacts in the hydroxide layers. These trends are consistent with the above assignments of the hydroxyl group resonances and, for MgAl-33, indicate that the Al and Mg cations must be ordered in the metal hydroxide sheets, as shown in Fig. 1C. Furthermore, as shown in Table 1, the experimental concentrations of the hydroxyl groups are in good agreement with the relative concentrations calculated using models that assumed Al-Al avoidance and thus the presence of only Mg_3-OH and Mg_2Al-OH hydroxyl groups. Differences between the experimental intensities and those calculated assuming Al-Al avoidance are ascribed to errors associated with the deconvolution of the ^{1}H NMR spectra and the accurate measurement of Al content by inductively coupled plasma methods (see SOM text for details).

To verify the spectral assignments, we acquired ^{1}H-^{27}Al transfer of population in double-resonance (TRAPDOR) NMR spectra (*30*) of all three samples (Fig. 3). This experiment uses the dipole interaction between ^{1}H and ^{27}Al, which scales as the cube of the through-space distance between the two nuclei. Thus, the most pronounced TRAPDOR effect is expected for the hydroxyl groups coordinated to Al. The TRAPDOR difference spectra of MgAl-19 and MgAl-25 are dominated by a broad resonance whose center of gravity is at ~2.3 ppm, consistent with its assignment to a Mg_2Al-OH group in the ^{1}H MAS spectra. A resonance at 3.5 ppm dominates the difference spectra of MgAl-33, and this shift to higher frequency of the Mg_2Al-OH resonance is again in agreement with the ^{1}H MAS data. The slight discrepancies (≤0.5 ppm) between the centers of gravity of the ^{1}H resonances in the single pulse and ^{1}H-^{27}Al TRAPDOR experiments is ascribed to the much slower spinning frequency used in the TRAPDOR experiments (5 kHz). This results in incomplete averaging of the homonuclear ^{1}H dipolar couplings and thus much poorer resolution of the individual resonances and a loss of signal intensity during the echo experiment, particularly for the strongly coupled ^{1}H spins. Slow motion may also result in some partial loss of signal intensity. The water resonance in these slow spinning spectra is now contained in the intense spinning sidebands spanning over 100 ppm. The most important conclusion from these data are that there are no additional resonances at

Table 1. A comparison of the relative hydroxyl intensities calculated for a random distribution of metals and for an ordered arrangement of cations, assuming Al-Al avoidance, with those determined experimentally from the deconvolution and integration of single-pulse ^{1}H MAS NMR spectra obtained at a spinning speed of 60 kHz. Resonances in the 0.8 to 1.5, and 2.4 to 3.6 ppm ranges contribute to the Mg_3-OH and Mg_2Al-OH local environments, respectively.

	Relative concentrations of hydroxyl groups (%)							
	Random cation distribution				Ordered model		Experimental data	
	Mg_3OH	Mg_2AlOH	$MgAl_2OH$	Al_3OH	Mg_3OH	Mg_2AlOH	Mg_3OH	Mg_2AlOH
MgAl-19	54	37	8	0.6	43	57	38(3)	62(3)
MgAl-25	42	42	14	2	25	75	20(3)	80(3)
MgAl-33	30	44	22	4	1	99	3(1)	97(1)

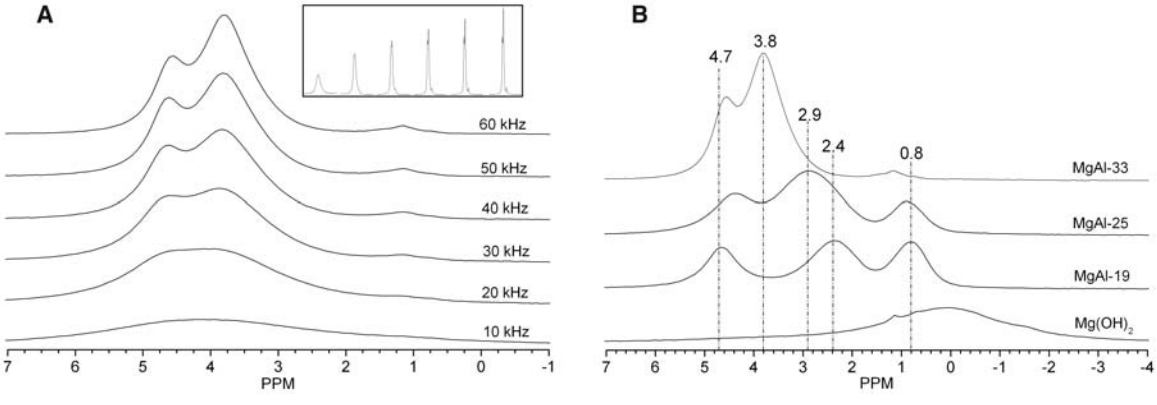

Fig. 2. (**A**) The ^{1}H MAS NMR spectra of MgAl-33 at 14 T as a function of spinning speed: Only the isotropic resonances are shown. The inset shows the same spectra side by side to emphasize the gain in resolution. (**B**) The effect of Al content on the single-pulse ^{1}H MAS NMR spectra collected at a spinning speed of 60 kHz. Hydrotalcite-like LDHs containing 19%, 25%, and 33% Al are shown. The very weak peak [less than 1% of the total signal for $Mg(OH)_2$] at ~1.2 ppm is due to ^{1}H background in the rotor from trace organic impurities (*22*).

higher frequencies, possibly obscured by the water resonance, which can be assigned to environments such as $MgAl_2$-OH.

The ^{25}Mg MAS NMR spectra of brucite, MgAl-19, MgAl-25, and MgAl-33 are shown in Fig. 4A. The spectrum of brucite is dominated by a resonance due to a single, axially symmetric $Mg(OMg)_6$ environment. This brucite-like [$Mg(OMg)_6$] resonance is present in the spectra of MgAl-19 and MgAl-25, but an additional component, associated with a larger quadrupolar coupling constant, is also observed, which grows in intensity with Al content. The $Mg(OMg)_6$ resonance is absent in the spectrum of MgAl-33, and only the second component is visible, which is again consistent with an axially symmetric Mg local environment.

We acquired TQ MAS NMR spectra to separate the different possible overlapping resonances. The ^{25}Mg TQ MAS NMR spectrum of MgAl-33 (Fig. 4B) clearly shows only one resonance, providing strong evidence that there is only one Mg local environment in this material and that no weaker resonances are hidden under the broad one-pulse spectrum. A projection of the anisotropic dimension was well simulated with the following NMR parameters: C_Q = 4.6 (±0.1) MHz, δ_{iso} = 13 (±2) ppm, η = 0.00 to 0.05; the slight line-shape distortion seen in the experimental spectrum is typical and reflects the orientation dependence of the TQ transition excitation efficiency. The measured C_Q is noticeably different from that of brucite, confirming that the ^{25}Mg electric-field gradient is extremely sensitive to Al substitution. The asymmetry parameter, η, is zero within the error limits, indicating that the Mg ions are in an axial environment, i.e., that there is a C_3 (or higher) rotational axis through the Mg atom. Furthermore, the presence of sharp discontinuities in the line shape implies that a negligible distribution of bond angles and bond lengths, associated with different local environments, is present, as such disorder would asymmetrically broaden the signal.

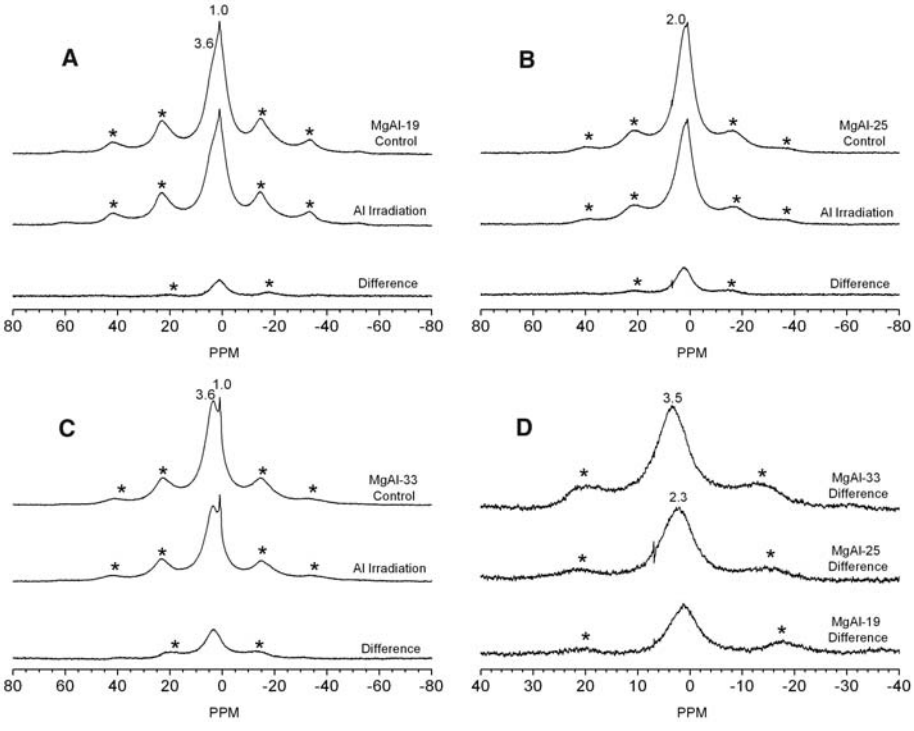

Fig. 3. Results of ^{1}H-^{27}Al TRAPDOR NMR experiments performed at 8.45 T at a spinning speed of 5 kHz for (**A**) MgAl-19, (**B**) MgAl-25, and (**C**) MgAl-33. The evolution and refocusing period of the spin-echo echo was set to one rotor period (0.2 ms) for all the measurements. The control (no Al irradiation, S_0), double-resonance (Al irradiation, S), and difference spectra (S_0–S), are shown from top to bottom in (A) to (C). A normalized comparison of the difference spectra for all three LDHs is shown in (**D**). * indicates spinning sidebands.

Only two local environments are consistent with C_3 symmetry, the brucite $Mg(OMg)_6$ environment and the $Mg(OMg)_3(OAl)_3$ environment found in the "honeycomb" ordering of Mg and Al (Fig. 1C). This ordering scheme results in only one local proton environment: Mg_2AlOH. The weak Mg_3OH resonance seen in the ^{1}H MAS NMR spectrum (accounting for 3% of the hydroxyl groups) of this sample suggests that some Mg-rich defects [e.g., $Mg(OMg)_6$ formed by replacing an Al^{3+} ion by a Mg^{2+} ion in the ordered, honeycomb sheets] are present in the sheets and that the Al content is slightly lower than 33%; these Mg environments are clearly present in too low a concentration to be observed in the TQ MAS spectrum. The ^{25}Mg TQ MAS spectra of the other two LDH samples contains more than one environment for Mg, consistent with their lower Al contents.

In conclusion, a combination of the ^{1}H MAS data and the ^{25}Mg TQ MAS data clearly shows that the Mg and Al cations are not randomly distributed in the LDH sheets and that in MgAl-33 they are ordered in a honeycomb arrangement. The ordering of the cations affects the charge density of the metal hydroxide sheets, which should have consequences regarding the bonding, reactivity, orientation, and mobility of the chemical species in the interlayer and on the sur-

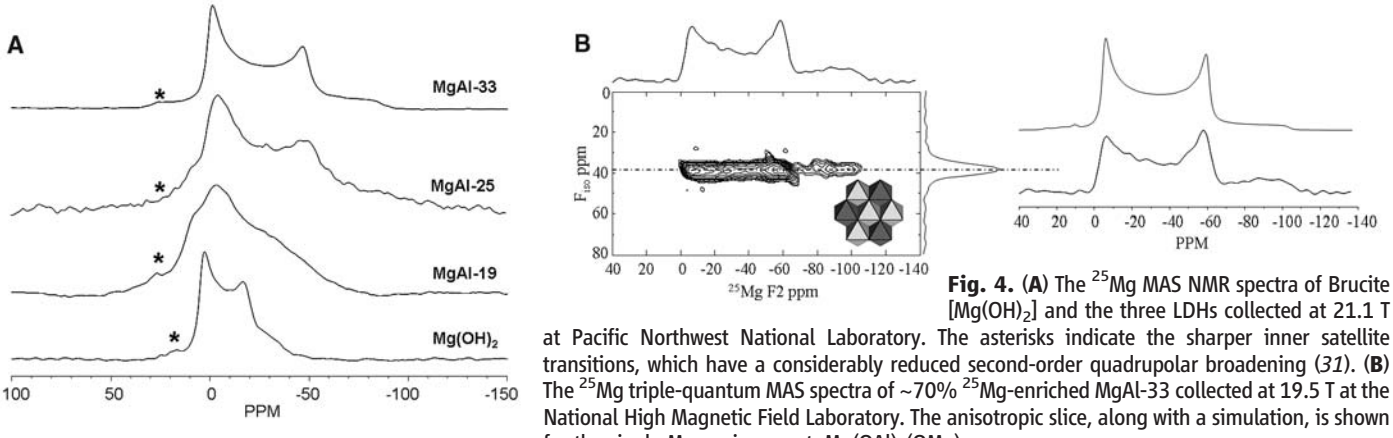

Fig. 4. (**A**) The ^{25}Mg MAS NMR spectra of Brucite [$Mg(OH)_2$] and the three LDHs collected at 21.1 T at Pacific Northwest National Laboratory. The asterisks indicate the sharper inner satellite transitions, which have a considerably reduced second-order quadrupolar broadening (*31*). (**B**) The ^{25}Mg triple-quantum MAS spectra of ~70% ^{25}Mg-enriched MgAl-33 collected at 19.5 T at the National High Magnetic Field Laboratory. The anisotropic slice, along with a simulation, is shown for the single Mg environment, $Mg(OAl)_3(OMg)_3$.

face. The results clearly demonstrate the power of rapid-spinning ^{1}H MAS NMR spectroscopy to resolve and quantify chemically distinct proton environments in hydrous minerals. This technology provides a simple brute-force method for studying strongly coupled multispin systems that should be straightforward to apply to a wide range of minerals. The approach can readily be used in conjunction with well-established 2D NMR or double-resonance experiments to determine, for example, the relationship between cation ordering and the binding affinities and dynamics of guest anions on the surfaces and in the interlayer spaces.

References and Notes

1. F. Cavani, F. Trifiro, A. Vaccari, *Catal. Today* **11**, 173 (1991).
2. V. Rives, M. A. Ulibarri, *Coord. Chem. Rev.* **181**, 61 (1999).
3. A. I. Khan, D. O'Hare, *J. Mater. Chem.* **12**, 3191 (2002).
4. D. Carriazo, M. del Arco, C. Martin, V. Rives, *Appl. Clay Sci.* **37**, 231 (2007).
5. X. Q. Hou, R. J. Kirkpatrick, *Chem. Mater.* **12**, 1890 (2000).
6. R. P. Bontchev, S. Liu, J. L. Krumhansl, J. Voigt, T. M. Nenoff, *Chem. Mater.* **15**, 3669 (2003).
7. U. Costantino, V. Ambrogi, M. Nocchetti, L. Perioli, *Micropor. Mesopor. Mat.* **107**, 149 (2008).
8. A. Vaccari, *Appl. Clay Sci.* **14**, 161 (1999).
9. F. Leroux, J. P. Besse, *Chem. Mater.* **13**, 3507 (2001).
10. W. Hofmeister, H. Von Platen, *Crys. Rev.* **3**, 3 (1992).
11. A. V. Radha, P. V. Kamath, C. Shivakumara, *Acta Crystallogr. B* **63**, 243 (2007).
12. M. A. Aramendia *et al.*, *J. Solid State Chem.* **131**, 78 (1997).
13. F. Rey, V. Fornes, J. M. Rojo, *J. Chem. Soc., Faraday Trans.* **88**, 2233 (1992).
14. A. Vanderpol, B. L. Mojet, E. Vandeven, E. Deboer, *J. Phys. Chem.* **98**, 4050 (1994).
15. J. Rocha, M. del Arco, V. Rives, M. A. Ulibarri, *J. Mater. Chem.* **9**, 2499 (1999).
16. K. J. D. Mackenzie, R. H. Meinhold, *Am. Mineral.* **79**, 250 (1994).
17. K. J. D. Mackenzie, R. H. Meinhold, B. L. Sherriff, Z. Xu, *J. Mater. Chem.* **3**, 1263 (1993).
18. T. J. Bastow, *Solid State Commun.* **77**, 547 (1991).
19. R. Dupree, M. E. Smith, *J. Chem. Soc. Chem. Commun.* **1988**, 1483 (1988).
20. K. J. D. Mackenzie, R. H. Meinhold, *Thermochim. Acta* **230**, 339 (1993).
21. Materials and methods are available as supporting material on *Science* Online.
22. J. P. Yesinowski, H. Eckert, G. R. Rossman, *J. Am. Chem. Soc.* **110**, 1367 (1988).
23. S. Sham, G. Wu, *Inorg. Chem.* **39**, 4 (2000).
24. C. V. Grant, V. Frydman, L. Frydman, *J. Am. Chem. Soc.* **122**, 11743 (2000).
25. N. G. Dowell, S. E. Ashbrook, S. Wimperis, *J. Phys. Chem. B* **108**, 13292 (2004).
26. L. Frydman, J. S. Harwood, *J. Am. Chem. Soc.* **117**, 5367 (1995).
27. J. He *et al.*, *Struct. Bond.* **119**, 89 (2006).
28. U. Sternberg, E. Brunner, *J. Magn. Res. Ser. A* **108**, 142 (1994).
29. J. Jeener, B. H. Meier, P. Bachmann, R. R. Ernst, *J. Chem. Phys.* **71**, 4546 (1979).
30. C. P. Grey, A. J. Vega, *J. Am. Chem. Soc.* **117**, 8232 (1995).
31. A. Samoson, *Chem. Phys. Lett.* **119**, 29 (1985).

32. Support was provided by the Center for Environmental Molecular Sciences, funded by NSF grant CHE-0021934. Single-pulse ^{25}Mg MAS NMR was performed in the Environmental Molecular Sciences Laboratory, a national scientific user facility sponsored by the Department of Energy's Office of Biological and Environmental Research and located at Pacific Northwest National Laboratory. The NMR facility at the National High Magnetic Field Laboratory is supported by NSF and the state of Florida (DMR-0084173). P.J.S thanks J. Ford and A. Palmer for helping with data collection and A. Reynolds for the synthesis of related materials. P.J.S acknowledges the Graduate Assistance in Areas of National Need (GAANN) Fellowship for financial assistance. U.G.N. acknowledges the Camille and Henry Dreyfus Postdoctoral Program in Environmental Chemistry for financial support.

Supporting Online Material

www.sciencemag.org/cgi/content/full/321/5885/113/DC1
Materials and Methods
SOM Text
Figs. S1 to S3
References

10 March 2008; accepted 12 May 2008
10.1126/science.1157581

Autophagy Is Essential for Preimplantation Development of Mouse Embryos

Satoshi Tsukamoto,[1]* Akiko Kuma,[1,2]† Mirei Murakami,[1] Chieko Kishi,[1] Akitsugu Yamamoto,[3] Noboru Mizushima[1,2]‡

After fertilization, maternal proteins in oocytes are degraded and new proteins encoded by the zygotic genome are synthesized. We found that autophagy, a process for the degradation of cytoplasmic constituents in the lysosome, plays a critical role during this period. Autophagy was triggered by fertilization and up-regulated in early mouse embryos. Autophagy-defective oocytes derived from oocyte-specific Atg5 (autophagy-related 5) knockout mice failed to develop beyond the four- and eight-cell stages if they were fertilized by Atg5-null sperm, but could develop if they were fertilized by wild-type sperm. Protein synthesis rates were reduced in the autophagy-null embryos. Thus, autophagic degradation within early embryos is essential for preimplantation development in mammals.

During the transition from oocyte to embryo, maternal proteins and RNAs are rapidly degraded and replaced by zygotic proteins and RNAs. Degradation of maternal RNAs is thought to be mediated by binding of regulatory proteins to the 3′ untranslated regions of target RNAs or by microRNAs (*1*, *2*). In contrast, the mechanisms by which maternal proteins are degraded remain poorly understood. In mammals, protein degradation accelerates shortly after fertilization and is apparent by the early two-cell stage (*3*). Early embryogenesis may rely on the maternal protein stores as nutrients. Several maternal proteins are degraded by the ubiquitin-proteasome system (*4*, *5*), but it is unknown whether macroautophagy (referred to as autophagy hereafter), another major degradation system, plays an important role during this period. During autophagy, a portion of cytoplasm is sequestered into an autophagosome; this then fuses with the lysosome, and the cytoplasm-derived materials are degraded (*6*–*10*). Autophagy is important for various physiological processes such as starvation adaptation and intracellular quality control.

To investigate whether autophagy occurs in fertilized oocytes, we used autophagy-indicator mice, in which green fluorescent protein (GFP)–fused LC3, a mammalian Atg8 homolog present on autophagosomes, is systemically expressed (*11*, *12*). We collected oocytes and embryos from superovulated GFP-LC3 female mice after mating with wild-type males (*13*). Although metaphase II (MII) oocytes showed almost no GFP-LC3 dots, a number of dots that represented autophagosomes appeared in fertilized embryos at the one- to four-cell stage (Fig. 1, A and B, and fig. S1A). Electron microscopy of two-cell embryos confirmed the presence of autophagic vacuoles (Fig. 1C and fig. S2). Induction of autophagy was also confirmed by LC3 conversion (*11*), which was increased in two-cell embryos relative to MII oocytes (Fig. 1D). Additionally, phosphorylation of S6 kinase was reduced after fertilization, which suggested that mTOR, a negative regulator of autophagy, was inactivated (fig. S3). Thus, formation of auto-

[1]Department of Physiology and Cell Biology, Tokyo Medical and Dental University, 1-5-45 Yushima, Bunkyo-ku, Tokyo 113-8519, Japan. [2]SORST, Japan Science and Technology Agency, Kawaguchi 332-0012, Japan. [3]Department of Bio-Science, Nagahama Institute of Bio-Science and Technology, Nagahama 526-0829, Japan.

*Present address: Laboratory Animal Sciences Section, National Institute of Radiological Sciences, Chiba 263-8555, Japan.

†Present address: Genome Research Institute, University of Cincinnati, Cincinnati, OH 45237, USA.

‡To whom correspondence should be addressed. E-mail: nmizu.phy2@tmd.ac.jp